

Quantum teleportation of optical images with frequency conversion

Liubov V. Magdenko, Ivan V. Sokolov

V. A. Fock Physics Institute, St.-Petersburg University, 198504 Stary Petershof, St.-Petersburg, Russia

Mikhail I. Kolobov

Laboratoire PhLAM, Université de Lille-1, F-59655 Villeneuve d'Ascq cedex, France

We describe a new version of continuous variables quantum holographic teleportation of optical images. Unlike the previously proposed [1, 2] scheme, it is based on the continuous variables quantum entanglement between the light fields of different frequencies and allows for the wavelength conversion between the original and the teleported images. The frequency tunable holographic teleportation protocol can be used as a part of light-matter interface in quantum *parallel* information processing and *parallel quantum memory*.

PACS numbers: 42.50.Dv, 42.30.Wb, 42.50.Lc

Continuous variables quantum teleportation allows to transfer an arbitrary quantum state of the electromagnetic field between two spatially separated systems via an exchange of classical information in combination with quantum entanglement shared by these systems. Initially the protocol of continuous variable teleportation was proposed theoretically [3, 4] and realized experimentally [5, 6] for a single spatial mode of the electromagnetic field. Recently this protocol was generalized theoretically to spatially multimode electromagnetic fields [1, 2]. The important feature of spatially multimode teleportation scheme is that it allows for simultaneous parallel teleportation of optical images (still or time-varying) containing large number of elements or pixels. The proposed scheme was called *holographic teleportation* because it resembles the conventional holography with an important difference that the reconstructed image is a quantum copy of the original one with fidelity that can be made close to unity. It is impossible to achieve high fidelity in holographic teleportation without sharing multimode quantum entanglement by the original and the target systems.

One of possible applications of quantum teleportation is the light-matter interface for quantum memory [7] for light which allows to record and store a quantum state of light on that of an atomic ensemble. The generalized spatially multimode teleportation scheme opens new perspectives for creation of a *parallel quantum memory* for parallel processing of quantum information. For an efficient interaction between the light wave and the atomic medium it is desirable to have a possibility for tuning the optical frequency of light to that of the atomic transition without changing the quantum state of the electromagnetic field. Let us mention a proposal of quantum frequency conversion [8] that was the first demonstration of quantum state transfer into different frequency. In recent experiment [9] quantum transfer of qubits was successfully demonstrated between photons of wavelength 1310 nm and 710 nm.

In this letter we describe a new version of holographic teleportation of optical images with *frequency conversion*.

This means that an input image, carried by a light wave with optical frequency ω_1 , is teleported to the output image at different optical frequency ω_2 with preservation of its original quantum state. Similar to the frequency-preserving quantum holographic teleportation, discussed in Refs. [1, 2], to obtain high fidelity in the teleported image one needs to create spatially multimode entanglement between the original and the target systems. In our case the source of spatially multimode entanglement between the input image at frequency ω_1 and the teleported image at frequency ω_2 is a type-I traveling-wave non-degenerate optical parametric amplifier (OPA).

The optical scheme of holographic teleportation with frequency conversion is shown in Fig. 1. An input image which is to be teleported from Alice to Bob, is described by a slowly-varying field operator $\hat{A}_1^{\text{in}}(\vec{\rho}, t)$, where $\vec{\rho} = (x, y)$ is a two-dimensional transverse coordinate. An input electromagnetic wave carrying this image is splitted into two secondary waves by a 50/50 beam splitter BS₁, and two quadrature components of these secondary waves are homodyne detected by two difference detectors using two local oscillators LO_x and LO_y, two 50/50 beam splitters BS₂ and BS₃, and four efficient CCD cameras with appropriate spatial resolution. The local oscillator waves have the same frequency ω_1 as the carrier frequency of the input image. The slow-varying difference photocurrent densities from these CCD cameras, containing information about spatio-temporal quantum fluctuations of the input image, are transmitted from Alice to Bob and are used for preparation of the output field $\hat{A}_2(\vec{\rho}, t)$. The multi-channel modulators M_x and M_y perform spatio-temporal modulation of a coherent wave with different carrier frequency ω_2 . This part of the scheme can be viewed as a classic non-stationary holography, where the reconstructing wave has different wavelength.

A key ingredient of our teleportation scheme is a pair of spatially-multimode EPR fields $\hat{E}_n(\vec{\rho}, t)$, $n = 1, 2$. Since an entanglement between different carrier frequencies is needed, the fields are created by a type-I traveling-wave non-degenerate OPA. The dichroic mirror M₁ reflects the

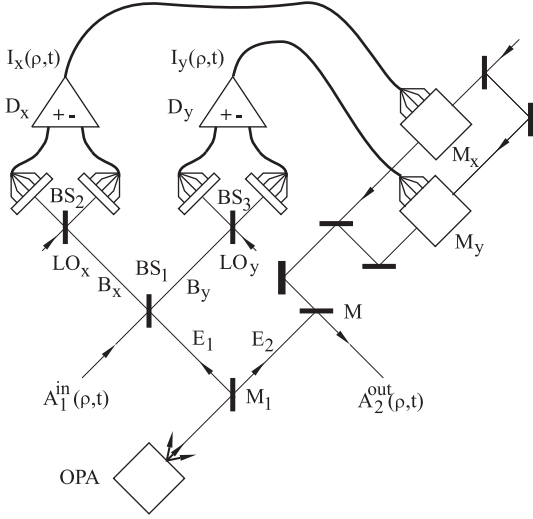


FIG. 1: Optical scheme of holographic teleportation with frequency conversion.

wave at frequency ω_1 and transmits that at frequency ω_2 . In the case of perfect reflectivity there are no frequency matched vacuum fluctuations entering from the open ports of M_1 into the corresponding fields.

Let us introduce slowly-varying spatio-temporal annihilation and creation operators $\hat{E}_n(\vec{\rho}, t)$ and $\hat{E}_n^\dagger(\vec{\rho}, t)$, $n = 1, 2$ of the electromagnetic waves with central frequencies ω_1 and ω_2 at the output of the non-degenerate OPA. The frequencies ω_1 and ω_2 obey the condition of energy conservation, $\omega_1 + \omega_2 = \omega_p$, where ω_p is the frequency of the pump wave. The field operators are normalized so that $\langle \hat{E}_n^\dagger(\vec{\rho}, t) \hat{E}_n(\vec{\rho}, t) \rangle$ gives the mean value of the irradiance, expressed in photons per cm^2 per second.

The transformation of the input fields $\hat{A}_n(\vec{\rho}, t)$ of the non-degenerate OPA in the vacuum state into the output fields $\hat{E}_n(\vec{\rho}, t)$ in the broadband multimode squeezed state is described in terms of the Fourier components of these operators in frequency and spatial-frequency domain, $\hat{E}(\vec{\rho}, t) \rightarrow \hat{e}(\vec{q}, \Omega)$. The squeezing transformation performed by a non-degenerate OPA, can be written as follows:

$$\hat{e}_n(\vec{q}, \Omega) = U_n(\vec{q}, \Omega) \hat{a}_n(\vec{q}, \Omega) + V_n(\vec{q}, \Omega) \hat{a}_{n'}^\dagger(-\vec{q}, -\Omega), \quad (1)$$

where $n = 1, 2$, $n \neq n'$, the coefficients $U_n(\vec{q}, \Omega)$ and $V_n(\vec{q}, \Omega)$ depend on the amplitude of the pump field, nonlinear susceptibility and the phase-matching condition. The explicit form of $U_n(\vec{q}, \Omega)$ and $V_n(\vec{q}, \Omega)$ can be found, for example, in Ref. [11]. The EPR correlations between the fields $\hat{E}_1(\vec{\rho}, t)$ and $\hat{E}_2(\vec{\rho}, t)$ are determined by two parameters, namely, the orientation angle $\psi_n(\vec{q}, \Omega)$ of the major axis of the squeezing ellipse [10] and the degree of squeezing $r_n(\vec{q}, \Omega)$,

$$\psi_n(\vec{q}, \Omega) = \frac{1}{2} \arg \{U_n(\vec{q}, \Omega) V_{n'}(-\vec{q}, -\Omega)\}, \quad (2)$$

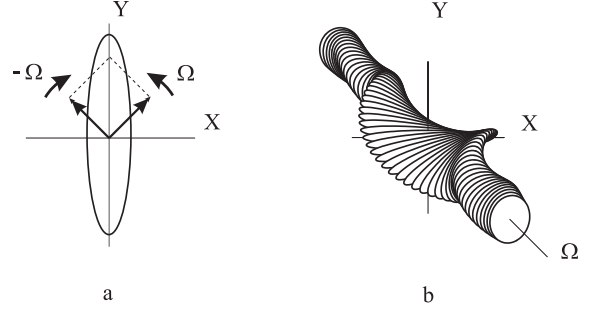


FIG. 2: Uncertainty region for the slow field amplitude from Eq. 4 (a), the frequency dispersion of squeezing ellipses for non-degenerate traveling-wave OPA, where $r_2(0, 0) = 3$, Ω – arb. units (b). Here X, Y – field quadrature components.

$$\exp[\pm r_n(\vec{q}, \Omega)] = |U_n(\vec{q}, \Omega)| \pm |V_{n'}(\vec{q}, \Omega)|. \quad (3)$$

It should be noted that in Fig. 1 we have chosen the input field at the frequency ω_1 and the output field at the frequency ω_2 , that corresponds to $n = 1$ and $n' = 2$ in Eqs. (2), (3), but with the same source of entangled beams the teleportation with frequency conversion can be performed from ω_2 to ω_1 as well.

It is instructive for better understanding of the scheme to give a simple physical explanation for the continuous variables quantum entanglement arising from squeezing in *non-degenerate* parametric down-conversion. For simplicity we shall omit the spatial dependence of the fields. Let us introduce the sum of two slow amplitudes, $\mathcal{E}(t) \sim E_1(t) + E_2(t)$ and consider a contribution to $\mathcal{E}(t)$ from a pair of Fourier amplitudes,

$$\mathcal{E}(t) \sim e_1(-\Omega)e^{i\Omega t} + e_2(\Omega)e^{-i\Omega t}. \quad (4)$$

One can show [12], that the discussed above squeezing ellipse for given Ω represents exactly the quantum uncertainty region for this contribution. For perfect squeezing this automatically implies a perfect phase matching beyond the classical limit between the slow amplitudes in the right side of (4), as illustrated in Fig. 2a. Let us remind that these amplitudes were defined with respect to the different carrier frequencies ω_1 and ω_2 . Hence the corresponding beams can be split by a dichroic mirror, preserving their quantum entanglement. The first slow amplitude is imprinted into the photocurrents by the homodyne detection and into the reconstructing field at different frequency ω_2 by the modulation. The second one *ab initio* is related to this frequency. A proper matching of the relative amplitudes and phases in quantum and classical channels leads to the quantum noise cancellation and effective teleportation.

Next important point is that the quantum modulation of the output field at a given frequency is now due to two independent pairs of entangled amplitudes, the first pair is shown in (4), another one corresponds to $\Omega \rightarrow -\Omega$. Therefore, in order to achieve optimal results one has to

take care of a proper phase matching of two independent squeezing ellipses (at Ω and $-\Omega$). The frequency dependence of squeezing within the frequency range of effective non-degenerate parametric down-conversion is graphically shown in Fig. 2b.

Apart from these new features, introduced by the frequency non-degenerate nature of the process, the fields evolution in the scheme is very similar to that described in Refs. [1, 2]. The input field $\hat{A}_1^{\text{in}}(\vec{\rho}, t)$ is mixed with one EPR beam $\hat{E}_1(\vec{\rho}, t)$ at the 50/50 beam splitter BS₁. The secondary waves \hat{B}_x and \hat{B}_y ,

$$\hat{B}_{x,y}(\vec{\rho}, t) = \frac{1}{\sqrt{2}}(\pm \hat{A}_1^{\text{in}}(\vec{\rho}, t) + \hat{E}_1(\vec{\rho}, t)), \quad (5)$$

with the $+$ ($-$) sign corresponding to x (y) channel, are photodetected by means of two balanced homodyne detectors. The difference photocurrents $I_x(\vec{\rho}, t)$ and $I_y(\vec{\rho}, t)$ collected from individual pixels of these matrices, carry the information about the spatio-temporal quantum fluctuations of the quadrature components of $\hat{B}_x(\vec{\rho}, t)$ and $\hat{B}_y(\vec{\rho}, t)$, phase matched with LO_{*x*} and LO_{*y*}. These photocurrents are sent from Alice to Bob via two multichannel classical communication lines and are used by Bob for spatio-temporal modulation of an external coherent wave with the frequency ω_2 , by means of two multichannel modulators M_x and M_y . The teleported field $\hat{A}_2^{\text{out}}(\vec{\rho}, t)$ is created by mixing of this modulated wave with a second EPR wave $\hat{E}_2(\vec{\rho}, t)$ at the mirror M with high reflectivity. By choosing appropriately the mirror transmission and the modulation depth, the teleported field $\hat{A}_2^{\text{out}}(\vec{\rho}, t)$ can be obtained as

$$\hat{A}_2^{\text{out}}(\vec{\rho}, t) = \hat{A}_1^{\text{in}}(\vec{\rho}, t) + \hat{F}(\vec{\rho}, t), \quad (6)$$

where $\hat{F}(\vec{\rho}, t)$ is an operator describing the noise added to the teleported field,

$$\hat{F}(\vec{\rho}, t) = \hat{E}_2(\vec{\rho}, t) + \hat{E}_1^\dagger(\vec{\rho}, t). \quad (7)$$

It can be demonstrated that the added noise can be considered as classical, thus preserving the commutation relations for the output field.

An ideal teleportation from ω_1 to ω_2 would correspond to the situation when the output field operator at different spatial points $\vec{\rho}$ and at different time moments t is an exact copy of the input field operator, $\hat{A}_2^{\text{out}}(\vec{\rho}, t) = \hat{A}_1^{\text{in}}(\vec{\rho}, t)$. However, as explained in Refs. [1, 2], this would require an infinite energy of the EPR beams and therefore could never be realized in practice. In real experimental situation the teleportation process will never take place “point-to-point”, but on average within some finite spatial area and within some finite time interval. In order to quantitatively describe the performance of our teleportation scheme we introduce a coarse-grained description of the input and output fields. Precisely, we consider the averaged field operator over a square pixel S_j of area

$S = \Delta^2$ and over a time interval T_i of duration T :

$$\hat{A}_2^{\text{out}}(j, i) = \frac{1}{\sqrt{ST}} \int_{S_j} d\vec{\rho} \int_{T_i} dt \hat{A}_2^{\text{out}}(\vec{\rho}, t), \quad (8)$$

with analogous definitions for the input field. The averaged field operators obey standard commutation relations of discrete field oscillators. The quadrature components of the averaged field operators at the output are

$$\begin{aligned} \hat{X}_\varphi^{\text{out}}(j, i) &= \hat{A}_2^{\text{out}}(j, i)e^{-i\varphi} + h.c., \\ \hat{Y}_\varphi^{\text{out}}(j, i) &= -i\hat{A}_2^{\text{out}}(j, i)e^{-i\varphi} + h.c., \end{aligned} \quad (9)$$

and similarly for the input field operators.

To characterize the noise added in the teleportation process we compare the correlation functions of the input and output quadrature components defined in Eq. (9). As follows from Eq. (6), the relation between these correlation functions is

$$\langle \delta \hat{X}_\varphi^{\text{out}}(j, i) \delta \hat{X}_\varphi^{\text{out}}(j', i') \rangle = \quad (10)$$

$$\langle \delta \hat{X}_\varphi^{\text{in}}(j, i) \delta \hat{X}_\varphi^{\text{in}}(j', i') \rangle + \mathcal{C}(j, j'; i, i'),$$

where $\mathcal{C}(j, j'; i, i')$ is the covariance matrix of the added noise. The explicit expression of this covariance matrix is

$$\mathcal{C}(j, j'; i, i') = 2 \int d\vec{q} \int d\Omega B_\Delta(\vec{q}) B_T(\Omega) \times \quad (11)$$

$$\cos[\vec{q} \cdot (\vec{\rho}_j - \vec{\rho}_{j'}) - \Omega(t_i - t_{i'})] G(\vec{q}, \Omega),$$

where $\vec{\rho}_j = \{x_j, y_j\}$ is the center of the j -th pixel, and t_i is the center of the i -th time interval. The functions $B_\Delta(\vec{q})$ and $B_T(\Omega)$ arise from the coarse-graining operation, and for a square pixel of size Δ they read,

$$\begin{aligned} B_\Delta(\vec{q}) &= \frac{\Delta^2}{4\pi^2} \text{sinc}^2\left(\frac{q_x \Delta}{2}\right) \text{sinc}^2\left(\frac{q_y \Delta}{2}\right), \\ B_T(\Omega) &= \frac{T}{2\pi} \text{sinc}^2\left(\frac{\Omega T}{2}\right). \end{aligned} \quad (12)$$

The Green function $G(\vec{q}, \Omega)$ expressed in terms of the orientation angle $\psi_2(\vec{q}, \Omega)$ and the degree of squeezing $r_2(\vec{q}, \Omega)$ from Eq. (2) looks like

$$G(\vec{q}, \Omega) = e^{2r_2(\vec{q}, \Omega)} \cos^2 \psi_2(\vec{q}, \Omega) + e^{-2r_2(\vec{q}, \Omega)} \sin^2 \psi_2(\vec{q}, \Omega). \quad (13)$$

As follows from Eqs. (11)-(13), the covariance matrix $\mathcal{C}(j, j'; i, i')$ is independent of the phase φ in Eq. (9). Thus, the added noise is the same for any quadrature.

In the absence of the EPR correlations, i. e. when $r_2(\vec{q}, \Omega) = 0$, we obtain the classical limit of teleportation with the covariance matrix $\mathcal{C}_{\text{cl}}(j, j'; i, i') = 2\delta_{jj'}\delta_{ii'}$. In this limit two units of vacuum noise are added at each

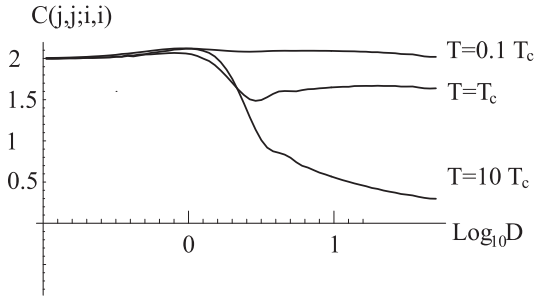


FIG. 3: Diagonal elements $\mathcal{C}(j, j; i, i)$ of the noise covariance matrix as a function of the relative pixel size $D = \Delta/l_c$ for three different observation times T equal to $10T_c$, T_c , and $0.1T_c$, here $r_2(0, 0) = 3$.

pixel exactly as for a single-mode teleportation and for the teleportation of images without frequency conversion.

Choosing the phase matching condition in the OPA such that $\psi_2(0, 0) = \pi/2$, we obtain reduction of the quantum noise below the standard quantum level within some bandwidth of spatial frequencies \vec{q} and temporal frequencies Ω determined by the phase-matching conditions in the crystal. When the pixel size Δ and the time window T are much larger than the characteristic coherence length l_c and the coherence time T_c of the OPA, we obtain

$$\lim_{\Delta \rightarrow \infty, T \rightarrow \infty} \mathcal{C}_{cl}(j, j'; i, i') = 2\delta_{jj'}\delta_{ii'} \exp[-2r(0, 0)]. \quad (14)$$

In Fig. 3 we illustrate the role of the pixel size Δ and of the integration time T in the teleportation process with frequency conversion. This figure shows the diagonal elements $\mathcal{C}(j, j; i, i)$ of the covariance matrix as a function of the relative pixel size $D = \Delta/l_c$ for three different observation times T equal to $10T_c$, T_c , and $0.1T_c$. The coherence time T_c for a frequency non-degenerate OPA is typically estimated as the time delay at the crystal length l between two wave packets centered at the frequencies ω_1 and ω_2 , $T_c \sim l|1/v_1 - 1/v_2|$, arising due to the difference of the group velocities v_n . Since a typical frequency spectrum of parametric down-conversion is fairly broad, a wave-packet spread due to the group velocity dispersion can also have an effect on squeezing and entanglement in our teleportation scheme, as we shall discuss elsewhere [12].

The frequency dependence of squeezing orientation angle, arising in a parametric crystal and illustrated in Fig. 2b, is a pure phase effect and can be compensated by propagation in a linear medium with a properly chosen frequency dependence of the refraction index. It is worth noting that in many interference experiments with twin photons, a need for similar compensation has been realized some time ago. Such a compensation can be applied to the plots shown in Fig. 3 and will be illustrated in the forthcoming publication [12].

The coherence time for a non-degenerate OPA is usually much larger than for a degenerate one. Therefore,

the assumption $T \gg T_c$ used in Refs. [1, 2] is not necessarily true anymore. The role of the observation time T is as crucial in the teleportation process as the role of the pixel size Δ . Indeed, as follows from Fig. 3, the diagonal elements of the covariance matrix which characterize the added noise power, decrease with growing pixel size Δ from the classical limit $\mathcal{C}(j, j; i, i) = 2$ to the EPR limit $\mathcal{C}(j, j; i, i) = 2 \exp[-2r(0, 0)]$ when the observation time is large compared with the coherence time T_c . However, when the observation time T becomes comparable with the coherence time T_c or smaller, the diagonal elements $\mathcal{C}(j, j; i, i)$ never reach the EPR limit but remain close to the classical limit even for large pixel size.

This results allow to estimate an effective number of spatio-temporal degrees of freedom for an input non-stationary image that can be teleported in our scheme.

In conclusion we have proposed a new scheme of quantum holographic teleportation of optical images from one optical frequency to another. We have presented preliminary analysis of the performance of our scheme and have revealed the possibilities to achieve high quality teleportation. More detailed calculations including evaluation of multi-pixel fidelity for this scheme are in progress and will be published elsewhere. This work was supported by the Network QUANTIM (IST-2000-26019) of the European Union and by the INTAS under Project No. 2001-2097. The research was performed within the framework of GDRE "Lasers et techniques optiques de l'information".

-
- [1] I. V. Sokolov, M. I. Kolobov, A. Gatti, and L. A. Lugiato, *Optics Communications*, **193**, 175 (2001).
 - [2] A. Gatti, I. V. Sokolov, M. I. Kolobov, and L. A. Lugiato, *Eur. Phys. J. D* **30**, 123 (2004).
 - [3] L. Vaidman, *Phys. Rev. A* **49**, 1473 (1994).
 - [4] S. L. Braunstein and H. J. Kimble, *Phys. Rev. Lett.* **80**, 869 (1998).
 - [5] A. Furusawa, J. L. Sorensen, S. L. Braunstein, C. A. Fuchs, H. J. Kimble, and E. S. Polzik, *Science*, **282**, 706 (1998).
 - [6] W. P. Bowen, N. Treps, B. C. Buchler, R. Schnabel, T. C. Ralph, H.-A. Bachor, T. Symul, and P. K. Lam, *Phys. Rev. A* **67**, 032302 (2003).
 - [7] B. Julsgaard, J. Sherson, J. Fiurasek, J. I. Cirac, and E. S. Polzik, *Nature* **432**, 482 (2004).
 - [8] J. Huang and P. Kumar, *Phys. Rev. Lett.* **68**, 2153 (1992).
 - [9] S. Tanzilli, W. Tillel, M. Halder, O. Alibart, P. Baldi, N. Gisin, and H. Zbinden, *Nature* **437**, 116 (2005).
 - [10] M. I. Kolobov, *Rev. Mod. Phys.* **71**, 1539 (1999).
 - [11] E. Brambilla, A. Gatti, M. Bache, and L. A. Lugiato, *Phys. Rev. A* **69**, 023802 (2004).
 - [12] L. V. Magdenko, M. I. Kolobov, and I. V. Sokolov (in preparation).